Research Article Vol. 1, No. 5 / November 2014 / Optica 356

Ultra-high-efficiency metamaterial polarizer

Bing Shen,[1] Peng Wang,[1] Randy Polson,[2] and Rajesh Menon[1,*]

[1]Department of Electrical and Computer Engineering, University of Utah, Salt Lake City, Utah 84112, USA

[2]Utah Nanofabrication Facility, University of Utah, Salt Lake City, Utah 84112, USA

*Corresponding author: rmenon@eng.utah.edu

Received 25 August 2014; revised 13 October 2014; accepted 14 October 2014 (Doc. ID 221615); published 20 November 2014

Conventional polarizers operate by rejecting undesired polarization, which limits their transmission efficiency to much less than 50% when illuminated by unpolarized light. We designed, fabricated, and characterized a multilevel metamaterial linear polarizer that rotates light with polarization perpendicular to its principal axis by 90 deg. Light with polarization parallel to its principal axis is transmitted undisturbed. Thereby, such a polarizer is able to output linearly polarized light from unpolarized input with a transmission efficiency that is substantially higher than the theoretical upper limit of 50%. A nonlinear optimization algorithm was used to design the polarizer, while multilevel focused-ion-beam lithography was used to fabricate it in silicon for the vacuum wavelength, $\lambda_0 = 1550$ nm. We experimentally confirmed that the fabricated device enhances the transmission of the desired linear polarization by 100% compared to an unpatterned film, corresponding to a transmission efficiency of ~74% at the design wavelength. Since our method allows for the generalized manipulation of the amplitude, phase, and polarization of light with high transmission efficiency using ultrathin elements, it should enable the efficient generation of complex vector distributions of light. © 2014 Optical Society of America

OCIS codes: (350.4238) Nanophotonics and photonic crystals; (050.1970) Diffractive optics; (350.3950) Micro-optics.

http://dx.doi.org/10.1364/OPTICA.1.000356

1. INTRODUCTION

Manipulation of the polarization of light is extremely important for a variety of applications ranging from communications [1] to imaging [2–4]. Conventional polarization selection devices (or polarizers) use absorption or reflection to discard the unwanted polarization [5]. In these polarizers, the maximum achievable transmission efficiency of the desired polarization is 50%. Commercial polarizers typically demonstrate transmission efficiencies that are lower [6]. In this article, we apply a new approach to designing a metamaterial polarizer that rotates one polarization by 90 deg, while the orthogonal polarization is transmitted undisturbed. Thereby, such a polarizer allows for substantially higher transmission efficiencies in the desired polarization. Furthermore, we show that our design methodology is applicable to metamaterials in general, and could enable unique and diverse photonic functions in lossless dielectric substrates.

Most conventional polarizers are based upon form birefringence [7] or total internal reflection effects in crystals or polymers, which cause phase retardation between the two orthogonal polarizations. Recently, a variety of novel approaches to polarization rotation have been proposed. Some of these employ surface gratings, whose scattering vectors are different from the polarization state of the incident light to achieve polarization manipulation [8,9]. Other devices achieve polarization manipulation using metasurfaces, i.e., carefully designed antennae that impart an abrupt phase change at an interface [10–12]. An alternative approach is to use subwavelength structures to manipulate polarization across a wavefront (inhomogeneous polarization) [13]. Polarization-manipulation devices have been utilized for a variety of applications [14–17]. Recently, these ideas have been generalized by combining conventional computer-generated holography [18] with subwavelength control for manipulation of the phase, amplitude, and polarization of light [19,20]. Related work described optical transmission by reflectionless metasurfaces. Polarization rotation of zero-order transmitted light through a perforated metal film was also recently demonstrated [21]. Experimental

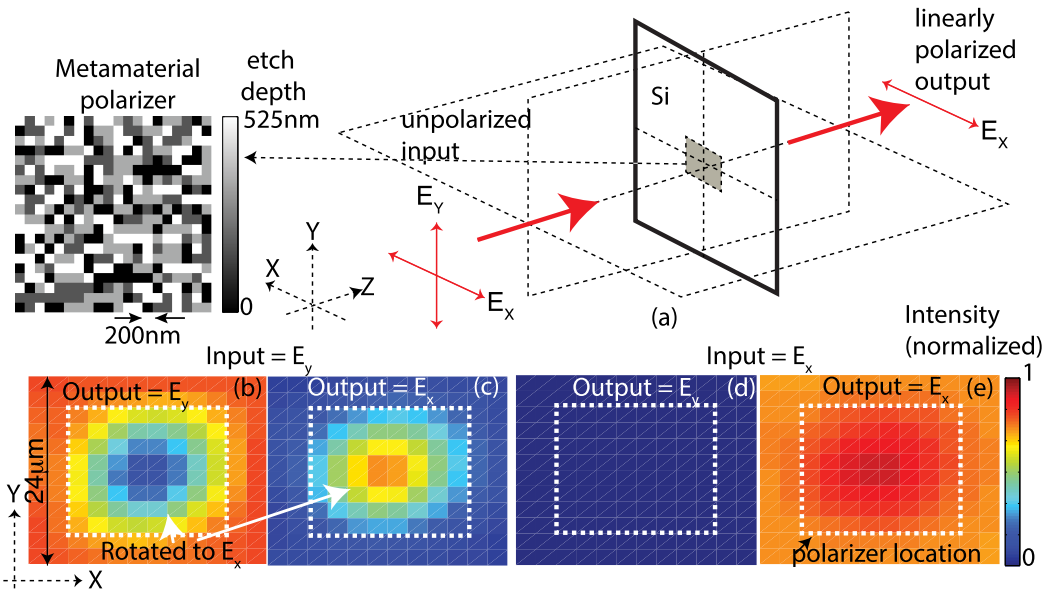

Fig. 1. (a) High-efficiency metamaterial polarizer. The design (left) is composed of etched square pixels in silicon. (b)–(e) Simulated light intensity distributions after transmission through the polarizer for (b) E_y and (c) E_x under E_y input and for (d) E_y and (e) E_x for E_x input. The white dashed lines in (b)–(e) indicate the boundaries of the finite device (Media 2, Media 3, Media 4, Media 5, Media 6, Media 7, Media 8, Media 9, Media 10, Media 11, Media 12, Media 13, Media 14, Media 15, Media 16, Media 17, Media 18, Media 19).

demonstration in the microwave regime was also given [22,23]. These approaches utilize metallic antennae on a single surface, which suffer from parasitic absorption. Nevertheless, only one polarization is manipulated in all previous devices, resulting in less than 50% transmission efficiency, when illuminated by both polarizations.

In contrast, our device is based upon an all-dielectric material that is patterned at subwavelength dimensions so as to enable independent manipulation of both polarizations. To illustrate the principle, we designed, fabricated, and characterized a metamaterial polarizer that operates by allowing one polarization to transmit undisturbed while rotating the orthogonal polarization.

2. DESIGN

Our design goal is to determine the etch depth of each pixel such that a desired phase, amplitude, and polarization distribution of light is obtained upon transmission through the device. We constrained our pixel size to 200 nm × 200 nm to enable fabrication. For computational expediency, we limited the device size to 20 × 20 pixels, corresponding to a total dimension of 4 μm × 4 μm. Furthermore, periodic boundary conditions were applied along the X and Y directions that allowed the unit to be repeated in 2D. We also constrained the maximum aspect ratio for ease of fabrication (Supplement 1).

The design was performed by a modified version of the direct-binary-search (DBS) algorithm. Previously, we have successfully utilized this algorithm to design nanophotonic light-trapping geometries [24,25] as well as broadband nonimaging diffractive optics [26–28]. Details of the algorithm are included in Supplement 1. Here, our optimization variables are the etch depths of each of the 200 nm × 200 nm pixels in our device. The algorithm attempts to maximize a figure of merit, which we define as the transmission efficiency at the desired polarization (E_x in Fig. 1), when the polarizer is illuminated by both polarizations (E_x and E_y) with equal amplitude. The optimized design is shown on the top left of Fig. 1(a). Although the design was performed using periodic boundary conditions, our fabricated device was composed of 4 × 4 unit cells (total size of 16 μm × 16 μm). In other words, the polarizer was surrounded by unpatterned silicon. We simulated the performance of this fabricated device and summarized the results in Figs. 1(b)–1(e) (see Supplement 1). When illuminated by collimated linearly polarized light with polarization along the Y axis (E_y source), the output light intensity in E_y decreases [Fig. 1(b)], while that in E_x increases as shown in Fig. 1(c). In other words, the input field oriented along the Y axis after propagation through the polarizer is substantially rotated such that it is oriented along the X axis. On the other hand, when the device is illuminated with light polarized along the X axis (E_x source), it transmits mostly undisturbed as shown in Figs. 1(d) and 1(e). Small perturbations of the fields in the output are due to diffraction at the boundary of the polarizer, where the periodic boundary conditions are not satisfied. Spatial nonuniformity of the transmitted fields is expected, since the unit cell does not exhibit any symmetry. We further confirmed using simulations that only 13% of the incident light is reflected, while 74% of the incident light is transmitted into the desired E_x polarization (Supplement 1). Compared to the surrounding unpatterned silicon, the transmission of E_x is enhanced by 110%, and the ratio of the transmitted power at E_x to that at E_y at the output is calculated to be 8.8.

3. EXPERIMENTS

The device was fabricated by etching into silicon using focused-ion-beam lithography using gallium ions. Different etch depths are achieved by varying the deposited energy or

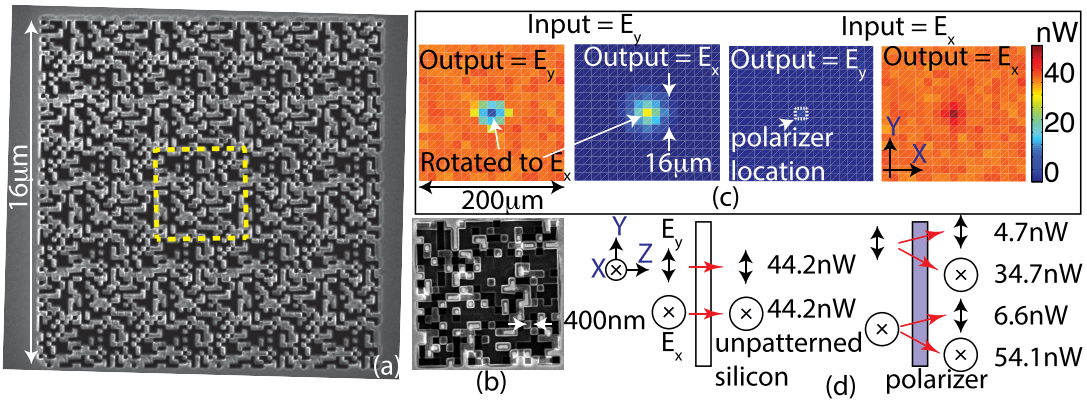

Fig. 2. (a) Scanning-electron micrograph of the metamaterial polarizer. One unit cell is 4 μm × 4 μm (yellow dashed lines). (b) Magnified view shows pixels with a period of 400 nm. (c) Measured transmitted power as a function of position in the X–Y plane. The left two images correspond to the E_y source, while the right two images correspond to the E_x source. Within the device area (dashed white square), E_y is rotated to E_x. (d) Comparison of the measured peak transmitted power in E_x and E_y between unpatterned silicon and the metamaterial polarizer.

exposure dose at each location (see Supplement 1). Figure 2(a) shows the scanning-electron micrograph of a fabricated device composed of 4 × 4 unit cells, where each unit cell is 4 μm × 4 μm (denoted by dashed yellow lines). A magnified view of one unit cell in Fig. 2(b) shows the multiple etch depths and the square pixels.

In order to characterize the polarizer, we illuminated it with collimated linearly polarized light from a 1550 nm laser (Hewlett Packard model No. 8168E). The transmitted power was measured using a lens and a photodetector from a spot of size 14 μm on the sample (Fig. S2 of Supplement 1). A conventional polarizer was placed at the output to measure the power at the two orthogonal polarizations separately. A half-wave plate and a polarizer were used at the input to first align the direction of polarization to the Y axis of the metamaterial polarizer. Then, the device was stepped in the X–Y plane using a stage, while the photodetector registered the transmitted signal. The resulting image is shown in Fig. 2(c). The dashed white square shows the location of the metamaterial polarizer. Behind the device, the power in the E_x polarization is dramatically increased while that in the E_y polarization is correspondingly reduced. The experiment was repeated after aligning the incident polarization to the X axis of our polarizer. As shown in Fig. 2(c), the transmitted power is almost entirely in the E_x polarization, since the electric field oriented along the X axis is transmitted undisturbed. Figure 2(d) schematically compares the transmitted power between the metamaterial polarizer and unpatterned silicon. When illuminated by both polarizations, the metamaterial polarizer transmits a total of 88.8 nW in E_x compared to just 44.2 nW for unpatterned silicon. This increase is primarily due to the incident power in E_y being rotated 90 deg into E_x upon transmission. The measured results agree well with the simulated enhancement of 110%. The measured ratio of the transmitted power at E_x to that at E_y at the output is 7.8, which agrees with the simulated value of 8.8.

4. DISCUSSION OF RESULTS

It has been reported that polarization rotation occurs when the scattering vector is different from the polarization of the incident light [8,9]. The scattering structure, defined by our design, consists of a large number of locally varying scattering vectors. The scattering vectors vary with position not only in the planes perpendicular to the propagation direction but also along the propagation direction. The transmitted light after the metamaterial polarizer is the superposition of light scattered from all these elements. The optimization process is thus attempting to create a distribution of scattering vectors such that the cumulative effect after transmission is that one polarization state (E_x) is allowed to pass through with low loss, while the orthogonal polarization state (E_y) is rotated by 90 deg. We analyzed the electric fields within the device and show that the rotation of the E_y modes is primarily due to the near-field coupling between multiple resonant-guided modes that are excited upon illumination, similar to what has been reported in photonic crystals [29,30]. By analyzing the time-averaged intensity distribution in each layer of our device (see Fig. S10 of Supplement 1), we can readily show that when illuminated by a source polarized along the Y axis, dipoles that are polarized along the X axis are excited at the corners of each isolated pillar in the first layer. Such dipoles then couple energy into the structures in the adjacent layers of the metamaterial polarizer. Eventually, the last (third) layer of the polarizer radiates energy into the far field, still maintaining the polarization along the X axis. This is further confirmed by analyzing the time-dependent field variation in the X–Z and Y–Z planes in the vicinity of the hot spots as discussed in Supplement 1 and as illustrated in Media 2–19.

It is interesting to note that there is an apparent decrease in entropy due to the conversion of randomly polarized input light into linearly polarized output with high efficiency [31]. This is not really true, since the decrease of the polarization degree of freedom is accompanied by a larger increase in the spatial frequencies of the output wavefront. In other words, although the incident light is collimated, the transmitted light radiates in multiple directions (see Fig. S10 of Supplement 1).

We also performed careful analysis of the tolerance of the metamaterial polarizer to fabrication errors (Supplement 1). We show that the devices are robust to fabrication errors

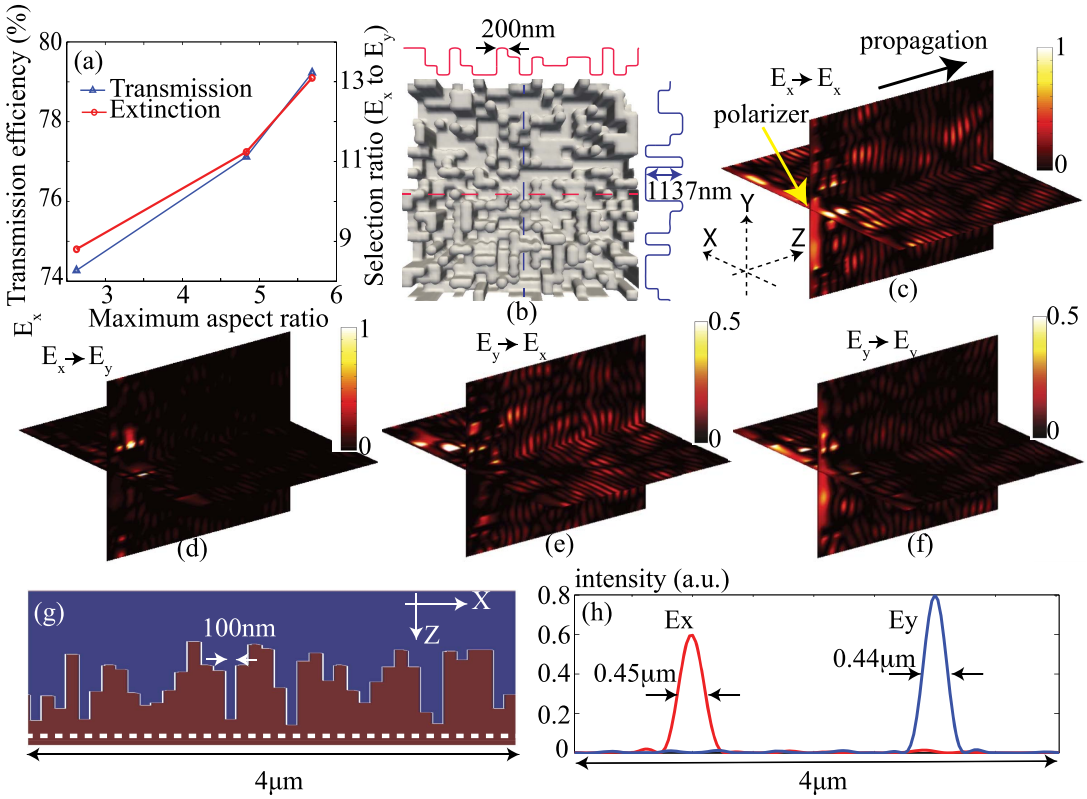

Fig. 3. (a) Transmission efficiency (at E_x) and selection ratio (power in E_x to power in E_y) as a function of maximum aspect ratio. (b) Device with transmission efficiency of 80% and maximum aspect ratio of 5.7. (c)–(f) Time-averaged intensity distributions after the device for (c), (d) E_x source and (e), (f) E_y source. The polarizer is located in the X–Y plane at the left edge. (g) 2D device designed for polarization separation and focusing. (h) Intensity distribution along the dashed white line in (g) when the device is illuminated by E_x and E_y simultaneously.

corresponding to about 8% of the pixel size. Small slopes in the sidewalls of the pixels also introduce only minor changes to the performance of the device. Although our device was designed for a single wavelength, we calculated the bandwidth to be ~20 nm (see Fig. S3 of Supplement 1). By incorporating a broadband source during design, it is possible to increase the device bandwidth further.

In order to ensure ease of fabrication, we applied a constraint on the maximum aspect ratio (defined as the ratio of the maximum etch depth to the pixel size). For the fabricated device, the maximum aspect ratio was 2.6. We performed a series of designs with higher maximum aspect ratios and realized that the performance of the device can be enhanced. Figure 3(a) shows the transmission efficiency at E_x and the selection ratio (power in E_x to power in E_y) as a function of the maximum aspect ratio. As the aspect ratio is increased, the transmission efficiency at E_x under unpolarized input can increase to almost 80%. The design for a maximum aspect ratio of 5.7 is shown in Fig. 3(b). The simulated electric-field distributions in the X–Z and Y–Z planes after transmission through the metamaterial polarizer are shown in Figs. 3(c) and 3(d) for the E_x source, and in Figs. 3(e) and 3(f) for the E_y source. Figures 3(c) and 3(e) show the electric-field distributions polarized along X, while Figs. 3(d) and 3(f) show the electric-field distributions polarized along Y. As expected, the polarizer rotates the incident E_y fields into E_x at the output, while the incident E_x fields transmit undisturbed. Note that no attempt was made to control amplitude in this case, and, hence, the transmitted intensity shows nonuniformity in the X–Y plane.

As we mentioned earlier, our design can be extended to control the phase, amplitude, and polarization of light. To demonstrate this capability, we designed a device that spatially separates and localizes fields according to their polarization in the plane normal to the direction of propagation (Supplement 1). In order to simplify the computation, this device was designed in 2D, and the optimized design is illustrated in Fig. 3(g). When this device is illuminated by an unpolarized source from above propagating from top to bottom, the electric fields are spatially separated along the X axis as shown by the intensity distributions in Fig. 3(h). The input field was uniform along the X axis for both polarizations. However, at the output, E_x becomes confined to a 0.45-μm-wide region on the left half (red line), while E_y is confined to a 0.44-μm-wide region on the right half (blue line). Note that this polarization separation is achieved within a propagation distance of only 1500 nm (less than the free-space wavelength of 1550 nm).

5. CONCLUSION

We designed, fabricated, and characterized a new metamaterial polarizer that rotates one polarization by 90 deg, while allowing the orthogonal polarization to transmit unperturbed.

We experimentally showed that this polarizer is able to enhance the transmission of one polarization by 100% compared to an unpatterned film. Appropriate design of these devices can achieve absolute transmission efficiencies at one desired polarization of almost 80% at the design wavelength (1.55 μm). Our approach is readily generalized to manipulate the phase, amplitude, and polarization state of electromagnetic fields at the subwavelength scale. The demonstrated device could have significant implications in imaging systems and displays (when extended to visible wavelengths). Although the extinction ratio for our device is smaller than conventional polarizers, the metamaterial polarizer could be useful where transmission efficiency is particularly important. Other interesting applications include the ability to efficiently generate complex modes that may be useful in quantum entanglement [32] and expanded bandwidth in telecommunications [33].

FUNDING INFORMATION

National Aeronautics and Space Administration (NASA) (NNX14AB13G); U.S. Department of Energy (DOE) (EE0005959); University of Utah.

ACKNOWLEDGMENT

We thank Jose Dominguez-Caballero for assistance with the direct-binary-search algorithm. Fruitful discussions with Eli Yablonovitch are gratefully acknowledged.

See Supplement 1 for supporting content.

REFERENCES

1. J. N. Damask, *Polarization Optics in Telecommunications* (Springer, 2004).
2. D. S. Kliger, J. W. Lewis, and C. E. Randall, *Polarized Light in Optics and Spectroscopy* (Academic, 1990).
3. V. V. Tuchin, L. V. Wang, and D. A. Zimnyako, *Optical Polarization in Biomedical Applications* (Springer, 2006).
4. Y. P. Svirko and N. I. Zheludev, *Polarization of Light in Nonlinear Optics* (Wiley, 1998).
5. S. W. Ahn, K. D. Lee, J. S. Kim, S. H. Kim, J. D. Park, S. H. Lee, and P. W. Yoon, "Fabrication of a 50 nm half-pitch wire grid polarizer using nanoimprint lithography," Nanotechnology **16**, 1874–1877 (2005).
6. Commercial polarizers in Thorlabs, http://www.thorlabs.us/newgrouppage9.cfm?objectgroup_id=4984.
7. R. C. Tyan, A. A. Salvekar, H. P. Chou, C. C. Cheng, A. Scherer, P. C. Sun, F. Xu, and Y. Fainman, "Design, fabrication, and characterization of form-birefringent multilayer polarizing beam splitter," J. Opt. Soc. Am. A **14**, 1627–1636 (1997).
8. N. K. Grady, J. E. Heyes, D. R. Chowdhury, Y. Zeng, M. T. Reiten, A. K. Azad, A. J. Taylor, D. A. R. Dalvit, and H. T. Chen, "Terahertz metamaterials for linear polarization conversion and anomalous refraction," Science **340**, 1304–1307 (2013).
9. J. Elliott, I. I. Smolyaninov, N. I. Zheludev, and A. V. Zayats, "Polarization control of optical transmission of a periodic array of elliptical nanoholes in a metal film," Opt. Lett. **29**, 1414–1416 (2004).
10. Y. N. Fang, P. Genevet, M. A. Kats, F. Aieta, J. P. Tetienne, F. Capasso, and Z. Gaburro, "Light propagation with phase discontinuities: generalized laws of reflection and refraction," Science **334**, 333–337 (2011).
11. F. Aieta, P. Genevet, N. Yu, M. A. Kats, Z. Gaburro, and F. Capasso, "Out-of-plane reflection and refraction of light by anisotropic optical antenna metasurfaces with phase discontinuities," Nano Lett. **12**, 1702–1706 (2012).
12. N. Yu, F. Aieta, P. Genevet, M. A. Kats, Z. Gaburro, and F. Capasso, "A broadband, background-free quarter-wave plate based on plasmonic metasurfaces," Nano Lett. **12**, 6328–6333 (2012).
13. S. Pancharatnam, "Generalized theory of interference, and its applications," Proc. Ind. Acad. Sci. A **44**, 247–262 (1956).
14. A. Niv, G. Biener, V. Kleiner, and E. Hasman, "Spiral phase elements obtained by use of discrete space-variant subwavelength gratings," Opt. Commun. **251**, 306–314 (2005).
15. A. Niv, G. Biener, V. Kleiner, and E. Hasman, "Propagation-invariant vectorial Bessel beams obtained by use of quantized Pancharatnam–Berry phase optical elements," Opt. Lett. **29**, 238–240 (2004).
16. G. Biener, A. Niv, V. Kleiner, and E. Hasman, "Geometrical phase image encryption obtained with space-variant subwavelength grating," Opt. Lett. **30**, 1096–1098 (2005).
17. G. Biener, A. Niv, V. Kleiner, and E. Hasman, "Near-field Fourier transform polarimetry by use of a quantized space-variant subwavelength grating," J. Opt. Soc. Am. A **20**, 1940–1948 (2003).
18. P. Hariharan, *Optical Holography: Principles, Techniques and Applications* (Cambridge University, 1996).
19. J. Lin, P. Genevet, M. A. Kats, N. Antoniou, and F. Capasso, "Nanostructured holograms for broadband manipulation of vector beams," Nano Lett. **13**, 4269–4274 (2013).
20. X. Ni, A. V. Kildishev, and V. M. Shalaev, "Metasurface holograms for visible light," Nat. Commun. **4**, 1–6 (2013).
21. S. Wu, Z. Zhang, Y. Zhang, K. Zhang, L. Zhou, X. Zhang, and Y. Y. Zhu, "Enhanced rotation of the polarization of a light beam transmitted through a silver film with an array of perforated S-shaped holes," Phys. Rev. Lett. **110**, 207401 (2013).
22. C. Pfeiffer and A. Grbic, "Metamaterial Huygens' surfaces: tailoring wave fronts with reflectionless sheets," Phys. Rev. Lett. **110**, 197401 (2013).
23. F. Monticone, N. M. Estakhri, and A. Alu, "Full control of nanoscale optical transmission with a composite metascreen," Phys. Rev. Lett. **110**, 203903 (2013).
24. P. Wang and R. Menon, "Optimization of generalized dielectric nanostructures for enhanced light trapping in thin-film photovoltaics via boosting the local density of optical states," Opt. Express **22**, A99–A110 (2014).
25. P. Wang and R. Menon, "Optimization of periodic nanostructures for enhanced light-trapping in ultra-thin photovoltaics," Opt. Express **21**, 6274–6285 (2013).
26. G. Kim, J. A. Dominguez-Caballero, and R. Menon, "Design and analysis of multi-wavelength diffractive optics," Opt. Express **20**, 2814–2823 (2012).
27. G. Kim, J. A. Dominguez-Caballero, H. Lee, D. Friedman, and R. Menon, "Increased photovoltaic power output via diffractive spectrum separation," Phys. Rev. Lett. **110**, 123901 (2013).
28. P. Wang and R. Menon, "Three-dimensional lithography via digital holography," in *Frontiers in Optics 2012/Laser Science XXVIII*, OSA Technical Digest (online) (Optical Society of America, 2012), paper FTu3A.4.
29. V. Liu, D. A. B. Miller, and S. Fan, "Ultra-compact photonic crystal waveguide spatial mode converter and its connection to the optical diode effect," Opt. Express **20**, 28388–28397 (2012).
30. J. Lu and J. Vučković, "Objective-first design of high-efficiency, small-footprint couplers between arbitrary nanophotonic waveguide modes," Opt. Express **20**, 7221–7236 (2012).
31. C. Brosseau, *Fundamentals of Polarized Light: A Statistical Optics Approach* (Wiley, 1998).
32. S. Franke-Arnold, L. Allen, and M. Padgett, "Advances in optical angular momentum," Laser Photonics Rev. **2**, 299–313 (2008).
33. N. Bozinovic, Y. Yue, Y. Ren, M. Tur, P. Kristensen, H. Huang, A. E. Willner, and S. Ramachandran, "Terabit-scale orbital angular momentum mode division multiplexing in fibers," Science **340**, 1545–1548 (2013).

59.64.129.225 {ts '2019-01-20 09:42:47'}